High-fidelity entangled-photon link for Quantum Key Distribution testbed

Giovanni Di Giuseppe[a], Alexander V. Sergienko[a,b], Bahaa E. A. Saleh[a], and Malvin C. Teich[a,b]

Quantum Imaging Laboratory
[a] Department of Electrical & Computer Engineering
[b]Department of Physics,
Boston University, 8 Saint Mary's St., Boston MA 02215

ABSTRACT

We report on the construction of polarization-entangled photon sources for quantum key distribution (QKD) testbed using nonlinear optical process of spontaneous parametric down-conversion (SPDC) pumped by a 266-nm and 351-nm continuous wave (cw) and a 415-nm femtosecond-pulsed laser sources. The efficient coupling of down-converted photons at 702 nm and 830 nm into optical single-mode fiber has enabled us to increase the rate of entangled-photon pairs available for transmission over communication channels with a high degree of polarization entanglement. The detection and characterization of the entangled-photon-state properties has been performed using commercially available Silicon avalanche photodiodes (APD) as well as using a novel photon-number-resolving cryogenic photodetector, which has been developed by our colleagues at the Boulder Division of NIST and brought to BU for tests with elements of the future DARPA Quantum Network.

Keywords: Quantum Key Distribution, Entanglement.

1. INTRODUCTION

We have previously demonstrated that the use of EPR states generated by type-II phase-matched spontaneous parametric down-conversion (SPDC) provides a richer range of entanglement options than does type-I SPDC.[1] In conjunction with coincidence (fourth-order) interferometry, it creates a more flexible, robust, and reliable quantum apparatus for cryptographic applications. The high contrast and stability of the fourth-order quantum interference patterns demonstrated in our initial experiments brings the performance of EPR-based quantum cryptography beyond the level of the best weak-coherent-state quantum cryptography systems.

Our use of a high-repetition-rate femtosecond-pulsed laser as a pump source significantly enhances the flux of entangled photon pairs available for key distribution. The down-converted entangled pairs appear only at well-defined times when pump pulses are present. A fixed 12.5-ns timing separation between consecutive pump pulses substantially improves the performance of single-photon detectors, increasing the high-fidelity detection rate. The available femtosecond timing helps significantly to develop gated operation of single-photon infrared detectors. To effectively transmit entangled photon sources through an optical fiber, we are engineering our sources to produce photons at wavelengths of 0.8, 1.3, and 1.55 μm. In addition, these sources must be effectively coupled into the fiber. Substantial progress in this direction has been made at 0.8 μm. We are also improving the intensity (rate) of the source, if possible up to 1 GHz, and developing a miniaturized source for field deployment.

Thus far, we have designed and demonstrated a high-fidelity source of entangled photons coupled into a single-mode optical fiber. It has been tested as a stand-alone component for integration into the quantum network.

Quantum Imaging Laboratory webpage: www.bu.edu/qil.
G.D.G. Also at: Istituto Elettrotecnico Nazionale *G. Ferraris*, Strada delle Cacce 91, I-10153 Torino, Italy. gdg@bu.edu
A.V.S.: E-mail: alexserg@bu.edu. Webpage: http://people.bu.edu/alexserg/.

Quantum Information and Computation, Eric Donkor, Andrew R. Pirich, Howard E. Brandt, Editors, Proceedings of SPIE Vol. 5105 (2003) © 2003 SPIE · 0277-786X/03/$15.00

2. FIBER-COUPLING OF HIGH-FIDELITY ENTANGLED PHOTON SOURCE

2.1. Spontaneous Parametric Down-Conversion

The use of spontaneous parametric down-conversion (SPDC) as a source of two-photon entangled states is attractive for its peculiarity, i.e. its reliability and high directionality in emission. In the process of nonlinear spontaneous parametric down-conversion, light from a pump laser beam is converted inside a non-linear optical crystal into sequences of highly correlated twin photons under the restrictions of the phase-matching conditions[2,3]:

$$\omega_s + \omega_i \approx \omega_p \qquad\qquad \mathbf{k}_s + \mathbf{k}_i \approx \mathbf{k}_p \,, \tag{1}$$

where ω_p and $\mathbf{k}_p$ are the angular frequencies and wave vectors (within the crystal) of the pump, and similarly $\omega_{s,i}$ and $\mathbf{k}_{s,i}$ refer to the down-converted output photons, indicated historically as signal (s), and idler (i). Since the photons are created in pairs as twins, the detection of one of them indicates, with certainty, the existence of the other. Furthermore, because of the phase-matching conditions, the direction and energy of a detected photon can be used to predict not only the existence, but also the direction and energy of the other photon of the pair. The process can be energy degenerate, in which case both daughter photons have the same energy; or non-degenerate, in which case the energy of the pump photon is split unequally among the two daughter photons. Thus one photon can be in the infrared frequency range while its twin is in the visible. Down-conversion is also said to be of type-I or type-II phase-matching depending on whether the photons in the pair have their polarizations parallel or orthogonal to one another.

The two-photon state generated in the SPDC process can be written

$$|\Psi\rangle = \int d\mathbf{k}_o \int d\mathbf{k}_e \, \tilde{\Phi}(\mathbf{k}_o, \mathbf{k}_e) \, \hat{a}_o^\dagger(\mathbf{k}_o) \, \hat{a}_e^\dagger(\mathbf{k}_e) |0\rangle \,, \tag{2}$$

where the suffixes o and e correspond, respectively, to ordinary and extraordinary polarizations, and the state function $\tilde{\Phi}(\mathbf{k}_o, \mathbf{k}_e)$ characterizes the coupling between the wave vectors:

$$\tilde{\Phi}(\mathbf{k}_o, \mathbf{k}_e) = \int d\mathbf{k}_p \, \tilde{E}_p(\mathbf{k}_p) \, \xi(\mathbf{k}_p - \mathbf{k}_o - \mathbf{k}_e) \, \delta(\omega_p - \omega_o - \omega_e) \,, \tag{3}$$

where $\tilde{E}_p(\mathbf{k}_p)$ represents the amplitude of the plane-wave expansion of the pump field, and $\xi(\mathbf{k}_p - \mathbf{k}_o - \mathbf{k}_e)$ represents the imperfect phase matching that results from the finite size of the parametric interaction volume.

2.2. Type-II Collinear Configuration with cw Pump @351nm

In the case of a collinear configuration of down-conversion output under type-II phase matching conditions, the polarization state of the two-photon is a product state $|o\rangle \otimes |e\rangle$. A scheme to generate a polarization-entangled state from a collinear type-II SPDC process is shown in Fig. 1. A beam splitter along the path of the two-photons splits them into the output paths (1 and 2). A beam splitter with a coincidence post-selection procedure allows a superposition of two amplitudes for which the photons with orthogonal polarization enter one in each output path of the beam splitter. If the two amplitudes are completely indistinguishable in their space-time modes, then the polarization is described by an entangled state

$$|o\rangle \otimes |e\rangle \qquad \Longrightarrow \qquad |o\rangle_1 \otimes |e\rangle_2 - |e\rangle_1 \otimes |o\rangle_2 \,. \tag{4}$$

The degree of entanglement in this case is related to the superposition of the two amplitudes, i.e. the joint probability amplitude to detect a photon in the path 1 at space-time location $(\mathbf{x}_1, t_1)$ and the other in the path 2 at space-time location $(\mathbf{x}_2, t_2)$. In the case of plane-wave cw pump field, those amplitudes can be written in a single mode theory as

$$\mathcal{A}_{1o,2e}(t,\tau)|o\rangle_1 \otimes |e\rangle_2 - \mathcal{A}_{2o,1e}(t,\tau)|e\rangle_1 \otimes |o\rangle_2 \,. \tag{5}$$

where $t = t_1 - t_2$, as expected for a stationary process such as the one generated with cw pump field, and

$$\mathcal{A}_{1o,2e}(t,\tau) = \mathcal{A}(t+\tau) \qquad\qquad \mathcal{A}_{2o,1e}(t,\tau) = \mathcal{A}(-t+\tau) \,. \tag{6}$$

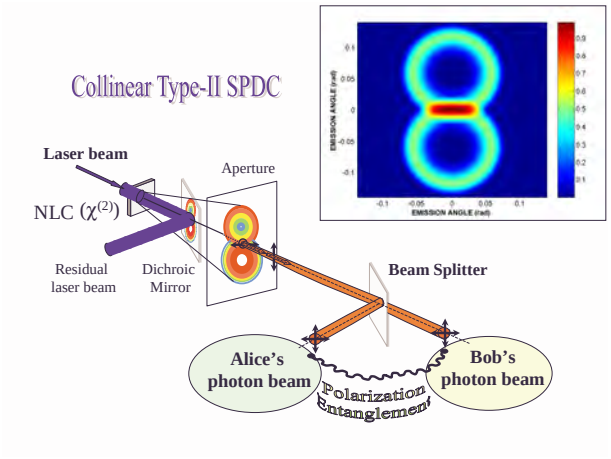

Figure 1. Generation of a polarization entangled state from a collinear type-II SPDC process. In the inset: emission angle in radians for degenerate (702-nm wavelength) collinear type-II SPDC in a 1-mm length crystal. The pump wavelength is 351 nm and the optical angle 48.9 deg.

The function $\mathcal{A}(t)$ is the Fourier transform of the state function $\tilde{\Phi}$ considered in the above approximation,

$$\tilde{\Phi}(\omega) = \mathrm{sinc}\left(\frac{DL\omega}{2}\right) \mathrm{e}^{-\mathrm{i}DL\omega/2} \qquad \mathcal{A}(t) = \Pi_{DL}(t)\,, \tag{7}$$

where $\Pi_{DL}(t) = 1$ for $0 \leq t \leq DL$ and zero otherwise.

A test of the polarization entanglement is the interference behavior of the fourth-order quantum interference, because even this effect is related to the superposition of the two amplitudes. It can be found that with polarization analyzer at 45 deg ($\pi/4$ rad) in the output path of the beam splitter, the coincidence rate shows a quantum interference pattern determined by

$$R_\tau(\tau, \pi/4, \pi/4) = R_0[1 - \mathcal{V}(\tau)]\,, \tag{8}$$

where R_0 accounts for the mean coincidence rate and the visibility function is given by:

$$\mathcal{V}(\tau) = \frac{\int dt\, \mathcal{A}^*(t+\tau)\mathcal{A}(-t+\tau)}{\int dt\, |\mathcal{A}(t)|^2} = \Lambda\left(\frac{2t}{DL} - 1\right)\,, \tag{9}$$

where $\Lambda(x)$ for $-1 \leq x \leq 1$. For a polarization analyzer directed along the axes at θ_1 and θ_2, the coincidence rate is

$$R_\tau(\tau, \theta_1, \theta_2) = R_0\{1 - \cos(2\theta_1 - 2\theta_2) + [1 - \mathcal{V}(\tau)]\sin(2\theta_1)\sin(2\theta_2)\}\,, \tag{10}$$

The maximum for the visibility function is 1 for $\tau = DL/2$; for this value $[V(DL/2) = 1]$ the polarization behavior is the same as for a polarization-entangled state.

In a more subtle theory of the SPDC two-photon state, the visibility function depends also on the characteristics of the optical elements that limit or manipulate the transverse wave vector reflecting the non-factorizable multi-parameter dependence of the state.[4, 5] This dependence becomes more important for single-mode fiber coupling of the SPDC, where any coupling mismatch represents a rapid decrease of the rate of the entangled state that one would want to share in a fiber link. For this purpose, we have analyzed fiber coupling. The coupling efficiency into two single-modes fiber with a fundamental field profile $\psi_j(\mathbf{x}, \omega)$ with $j = (1, 2)$, is

$$\eta_{fc} = \frac{P_{1,2}}{\sqrt{P_1\, P_2}}\,, \tag{11}$$

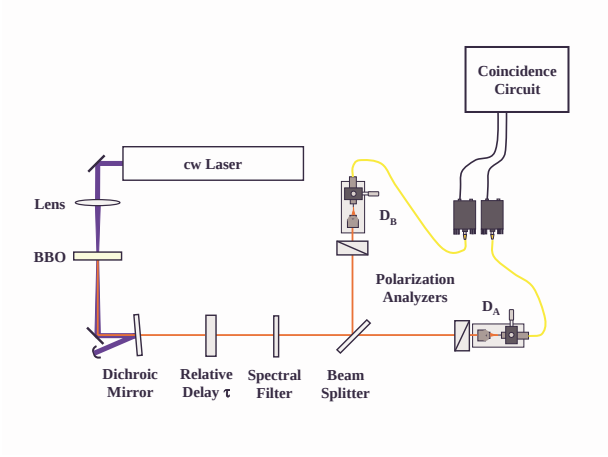

Figure 2. Experimental setup for collinear phase matching.

where

$$P_{1,2} = \int d\omega_o d\omega_e \left| \int d\mathbf{x}_1 d\mathbf{x}_2 \psi_1(\mathbf{x}_1,\omega_o)\psi_2(\mathbf{x}_2,\omega_e)\tilde{\mathcal{A}}_{1,2}(\mathbf{x}_1,\omega_o;\mathbf{x}_2,\omega_e)\right|^2 , \tag{12}$$

and

$$\begin{aligned} P_1 &= \int d\omega_o d\omega_e \int d\mathbf{x}_2 \left| \int d\mathbf{x}_1 \psi_1(\mathbf{x}_1,\omega_e)\tilde{\mathcal{A}}_{1,2}(\mathbf{x}_1,\omega_o;\mathbf{x}_2,\omega_e)\right|^2 \\ P_2 &= \int d\omega_o d\omega_e \int d\mathbf{x}_1 \left| \int d\mathbf{x}_2 \psi_2(\mathbf{x}_2,\omega_e)\tilde{\mathcal{A}}_{1,2}(\mathbf{x}_1,\omega_o;\mathbf{x}_2,\omega_e)\right|^2 . \end{aligned} \tag{13}$$

The amplitude $\tilde{\mathcal{A}}_{1,2}(\mathbf{x}_1,\omega_o;\mathbf{x}_2,\omega_e)$ is given by[6,7]

$$\tilde{\mathcal{A}}_{1,2}(\mathbf{x}_1,\omega_o;\mathbf{x}_2,\omega_e) = \int d\mathbf{q}_o d\mathbf{q}_e \tilde{\Phi}(\mathbf{q}_o,\omega_o;\mathbf{q}_e,\omega_e)\, H_1(\mathbf{x}_1;\mathbf{q}_o,\omega_o)\, H_2(\mathbf{x}_2;\mathbf{q}_e,\omega_e)\,. \tag{14}$$

The function $H_j(\mathbf{x}_j;\mathbf{q},\omega)$ is the Fourier transform of the transfer function $h_j(\mathbf{x}_j;\mathbf{x},\omega)$ $(j=1,2)$ for the propagation from the crystal through the lens to the fiber plane, and $\tilde{\Phi}(\mathbf{q}_o,\omega_o;\mathbf{q}_e,\omega_e)$ is the same function as in Eq. (3) when we specify the wave vectors $\mathbf{k}$ in terms of $(\mathbf{q},\omega)$.

Assuming that ideal f-lenses (thin and with infinite aperture) are placed at a distance d from the output plane of the crystal and image this plane with the fiber planes at distance b from the lenses, so that $1/d+1/b=1/f$, the transfer function can be written as

$$h_j(\mathbf{x}_j;\mathbf{x},\omega) = \mathrm{e}^{\mathrm{i}kd(1-1/\mu)}\, \mathrm{e}^{\mathrm{i}\frac{k}{2d}\mu(\mu-1)|\mathbf{x}|^2}\, \delta(\mathbf{x}-\mu\mathbf{x}_j)\,, \tag{15}$$

where $\mu = d/f-1$. Using Eq. (15) in Eq. (14) we obtain $\tilde{\mathcal{A}}_{1,2}(\mathbf{x}_1,\omega_o;\mathbf{x}_2,\omega_e) \sim \Phi(\mu\mathbf{x}_1,\omega_o;\mu\mathbf{x}_2,\omega_e)$. The coupling efficiency is a measure of the overlap of the function $\Phi(\mu\mathbf{x}_1,\omega_o;\mu\mathbf{x}_2,\omega_e)$, the inverse 2D-Fourier transform respect to $(\mathbf{q}_o,\mathbf{q}_e)$ of $\tilde{\Phi}(\mathbf{q}_o,\omega_o;\mathbf{q}_e,\omega_e)$, representing the coupling between the wave vectors into the crystals (see insets in Fig. 1 and 5), and the field profile of the single-mode fibers.

Figure 2 shows the experimental setup for our collinear configuration. A 200-mW cw Ar^+-ion laser operated at 351.1 nm served as the pump. This highly monochromatic laser beam was focused with a UV-lens with f = 1 m and passed through a beta-barium-borate (BBO) crystal with thickness 0.5 mm, placed in the region of minimum

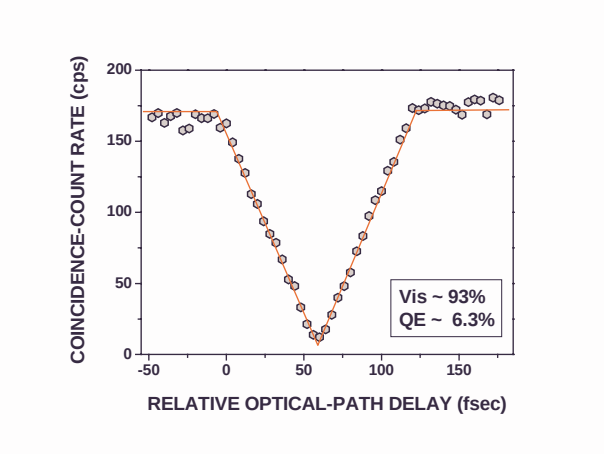

Figure 3. Fourth-order quantum interference pattern with polarization analyzers at 45 deg. The visibility is 93% and the overall quantum efficiency (optical losses, fiber coupling and detector efficiency) is 6.3%.

beam waist ∼100 mm. The crystal was aligned to produce pairs of orthogonally polarized photons by degenerate collinear type-II spontaneous parametric down-conversion. A dichroic mirror, which transmits the 702-nm signal and idler beams while reflecting the 351-nm pump, was placed after the two crystals to remove residual pump laser beam. A relative optical-path delay τ was introduced using a z-cut birefringent crystalline-quartz plate of variable thickness. The beams of down-converted light were then directed to a non-polarizing beam splitter, and then to the two arms of a polarization intensity interferometer. Each arm of the interferometer comprised a Glan-Thompson polarization analyzer set at 45 deg with respect to the horizontal axis in the laboratory frame, establishing the basis for the polarization measurements. This basis was selected so as to permit observation of the quantum-interference pattern as a function of the optical-path delay τ. Finally, achromatic lenses were used to map geometrically the incoming modes to the receiving modes of a single-mode optical fiber at 1.3/1.55 μm (Newport F-SS/F-SS-C) with a mode field diameter of $w_f = 9.3$ μm . The FC-output of fiber pigtails were FC-connected to two detectors, actively quenched Peltier-cooled photon-counting avalanche photodiodes (Perkin Elmer SPCM-AQR14). To reduce the background a wide bandwidth, FWHM = 70nm, spectral filters at 702 nm wavelength were used. Coincidence detection was performed using a 3-nsec integration window. In Fig. 3, we show the result of our experiment for the polarization entanglement test. The visibility obtained was 93% and the overall quantum efficiency (optical losses, fiber coupling and detector efficiency) was 6.3%.

The data for a polarization test for the configuration of Fig. 2 is shown in Fig. 4. The coincidences rates are reported in function of the angle of the polarization analyzer when both the polarization analyzers are rotated according to the two constrains $\theta_1 + \theta_2 = 0$ and $\theta_1 - \theta_2 = 0$. The two curves are consistent with the predictions of Eq. (10) with a visibility of 89%.

2.3. Type-I Non-Collinear Configuration with cw Pump @266nm

It is possible derive an analytic solution of the coupling efficiency, assuming gaussian pump field with a beam radius r_p into the crystal as wells as single-mode field profile defined by the parameter w =MFD/$2\sqrt{2}$ where MFD is the mode-field-diameter (see Fig. 5). With these approximations, the coupling efficiency is found to be

$$\eta_{\rm fc} = 4\frac{(1+\xi^2)}{(2+\xi^2)^2}\,\frac{\mathrm{erf}(\sigma_c)}{\sigma_c}\sqrt{\frac{\sigma_1}{\mathrm{erf}(\sigma_1)}\frac{\sigma_2}{\mathrm{erf}(\sigma_2)}} \tag{16}$$

where $\xi = w\mu/r_p$ and

$$\sigma_c = \frac{L}{r_p}\sqrt{\frac{(\alpha_1+\alpha_2)\xi^2+\beta}{\xi^2(2+\xi^2)}} \qquad\qquad \sigma_j = \frac{L}{r_p}\sqrt{\frac{\alpha_j}{1+\xi^2}} \tag{17}$$

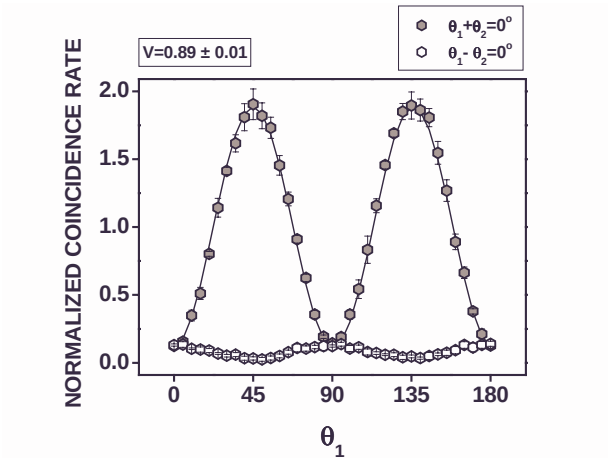

Figure 4. Polarization measurements. The fourth-order patterns show the entanglement in polarization of the state generated according to the configuration of Fig. 2. The measurements obtained assuming $\theta_1 = -\theta_2$ and $\theta_1 = \theta_2$ are consistent with the prediction of Eq. (10).

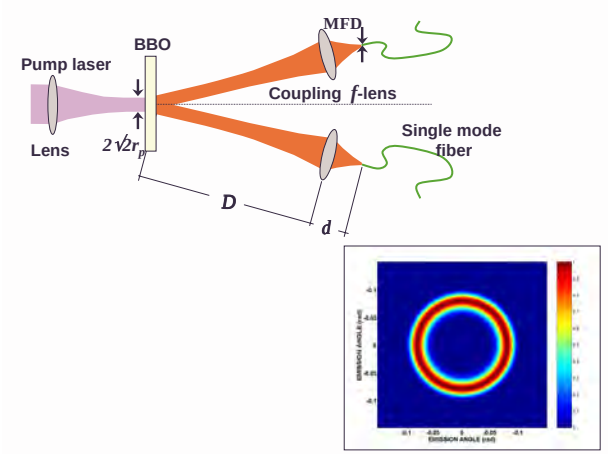

Figure 5. Sketch of the fiber coupling experiment. In the inset: emission angle in radians for degenerate (532-nm wavelength) non-collinear type-I SPDC in a 1-mm length crystal. The pump wavelength is 266 nm and the optical angle 48.2 deg.

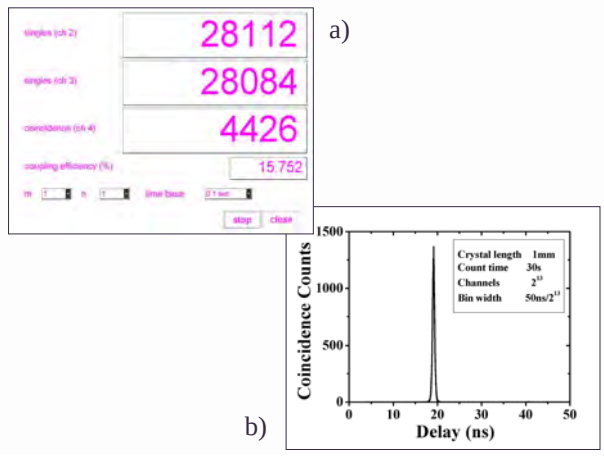

Figure 6. a) Print-screen showing the singles and coincidence rates in the experiment with a Type-I SPDC. The maximum overall efficiency obtained was 15.75%. Assuming detector QE 50% and filters transmission coefficients of 90% we can estimate a coupling efficiency of around 35%. The coincidences rate is 270 cps/mm(BBO)/mW(pump). b) MCA output.

L is thickness of the non-linear crystal and α_1 and β are parameters determined only by the birefringent properties of the crystal and the phase matching conditions. The parameter ξ is defined as $\xi = w\mu/r_p$ where $\mu = \mathcal{D}/d = \mathcal{D}/f - 1$ is the inverse of the magnification of the optical systems constituted by the fiber coupling lenses with focus length f. The validity of the expression for the coupling efficiency has been experimentally checked using a cw pump at 266nm. Entangled photons have been generated in a non-collinear Type-I configuration using a BBO crystal cut for at θ =47.7 and slightly tilted. The inset in Fig. 5 shows the calculated emission angles of the degenerate process (both photons @532nm) for a 1mm crystal length and a pump angle of 48.2°.

The pump beam with a power of 16.5 mW was focused with a 50cm-lens to a diameter of around 100mm into a 0.5mm-length BBO crystal and the SPDC photons generated was collected using 6.2mm coupling lenses (f) into a singel-mode fibers @532nm (MFD 3.3μm). The distance between crystal and coupling lenses was about 35cm. In Fig. 6a is showed the singles as well the coincidences rates observed. The coincidence rate can be quantified as 270 cps/mm(BBO)/mW(pump). A typical MCA output is shown in Fig. 6b.

The singles and the coincidence counts when one fiber is scanned with computer-controlled piezo translators are shown in Fig. 7. A maximum coupling efficiency of 15.75% was obtained after that a pump beam selection through a spatial filter. Without the spatial selection, the shapes of the singles and coincidence counts reflect the asymmetry of the pump beam profile. The pump beam asymmetry introduces a reduction of visibility due to the imperfect superposition between fiber mode and imaged pump beam profile as dictated by Eqs. (12) and (14).

2.4. Type-II Non-Collinear Configuration With Femtosecond-Pulsed Pump @415nm

In the case of a non-collinear configuration of type-II SPDC, it is possible to select correlated modes that are in a polarization-entangled state. For an opportune angle of the optical axes with respect to the pump-beam direction, the two emission cones, ordinary and extraordinary, can overlap as shown in Fig. 8.

To optimize polarization entanglement in the degenerate non-collinear process the angle of the optical axes should be chosen so that the emission region for the polarization entangled state has maximum symmetry, i.e. to have orthogonal intersection of the two-emission cone, allowing better fiber coupling. This is shown in the inset of Fig. 8, where for a pump wavelength of 415 nm the angle of the optical axes is 41.6 deg which has an emission angle for optimum emission at ~3.8deg.

The space-time indistinguishability of the two amplitudes was realized with a compensation system in only one arm comprised of a $\lambda/2$ plate and an equal-length BBO crystal, i.e. 0.5 mm in our case. In the other arm, we

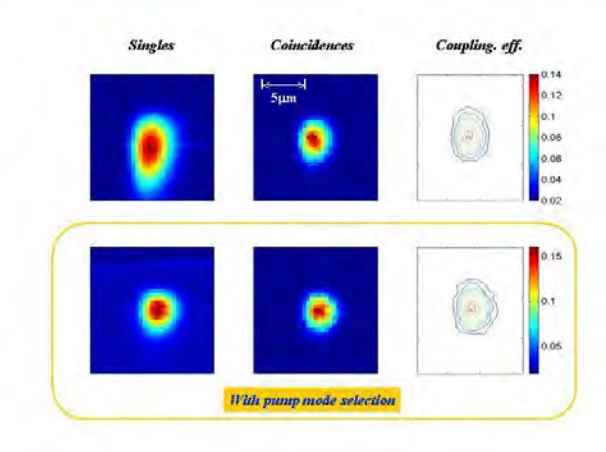

Figure 7. Scans of the singles and coincidence count rates when one of the fibers is maintained fixed shown the relevance of the pump beam profile.

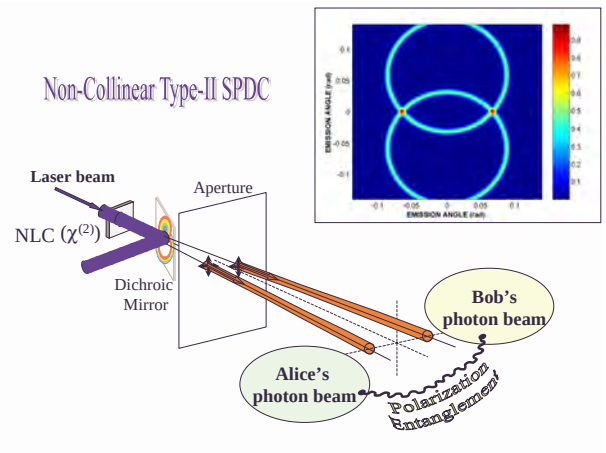

Figure 8. Sketch of the generation of a polarization entangled state in a non-collinear SPDC process. In the inset: emission angle in radians for degenerate (830-nm wavelength) non-collinear type-II SPDC in a 3-mm length crystal. The pump wavelength was 415 nm and the angle of the optical axes 41.6 deg. The emission angle for the polarization entangled state is ∼3.8deg. This value is chosen to have maximal symmetry in the entangled region, i.e. to have an orthogonal intersection of the two-emission cone, for better fiber coupling.

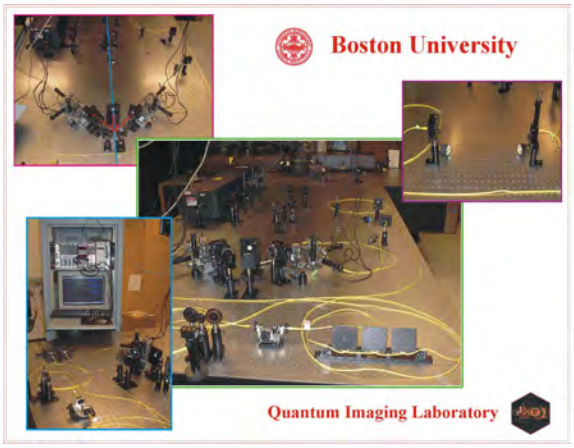

Figure 9. Experimental setup for non-collinear phase matching configuration @415nm.

also used a $\lambda/2$ plate to restore the proper state. The beams of down-converted light were then directed trough a Glan-Thompson polarization analyzer. Achromatic lenses were used to geometrically map the incoming modes to the receiving modes of a single-mode optical fiber with a mode field diameter of MFD ∼5 mm at 830 nm. The FC-output of the fiber pigtails were FC-connected to two detectors, actively quenched Peltier-cooled photon-counting avalanche photodiodes (PerkinElmer SPCM-AQR14). In Fig. 9, we show the experimental setup for coupling the SPDC into single-mode fibers at 830 nm, generated by 50 mW mean power from a pulsed pump at a wavelength of 430 nm and mode-locked at 76 MHz. The UV beam was focused with a lens with 50-cm focal-length into a 0.5-mm-thick BBO crystal. The beam waist was ∼60 mm. To reduce the background, wide bandwidth (FWHM=70 nm) spectral filters at 830 nm wavelength were used. Coincidence detection was performed using a 5-nsec integration window. To determine whether the pump pulse was below the value allowing high probability of double-pair emission, we measured the time correlation of the SPCM output with a standard TAC/Counter technique. The background for the coincidence count was found to be $> 1\%$ (see Fig. 10a). As shown in Fig. 10a and 11, the overall coupling obtained was 25.9%, which, accounting for the 50% quantum efficiency of the detectors and the $\sim$ 90% transmission of the spectral filters, corresponds to a ∼58% coupling efficiency and optical losses. In Fig. 12, we report results of a Bell-like-state analysis performed with one polarization analyzer at 45 deg while rotating the other. The visibility (∼98%) confirms the high quality of the resulting polarization entangled state can be obtained with this setup.

3. HIGH-QUALITY SINGLE-PHOTON DETECTION

3.1. Single-Photon Avalanche Photodiode

The detectors used in both experiments were commercially available actively quenched Peltier-cooled photon-counting avalanche photodiodes (SPCM-AQR14) with an FC-connector manufactured by PerkinElmer. The output signal is a standard TTL pulse. The maximum QE ∼73% is at about 700 nm. Typical dark counts are ∼50 cps, the single-photon time resolution is ∼350 ps at FWHM, and the dead time ∼50 ns with a maximum rate of ∼10 Mcps.

3.2. Photon-Number Resolving Detection

We have demonstrated the operability in our system of a new detector that is capable of resolving the detection of one photon from two or more (2,3,4,5,..) in quantum interferometry. This single-photon counting device is based on the superconducting transition-edge sensor (TES) technology currently being developed for photon-counting that stretches from the gamma-ray region all the way down to the near-infrared. Our colleagues at the Boulder Division of NIST have designed and fabricated TES photon counters and have optimized their

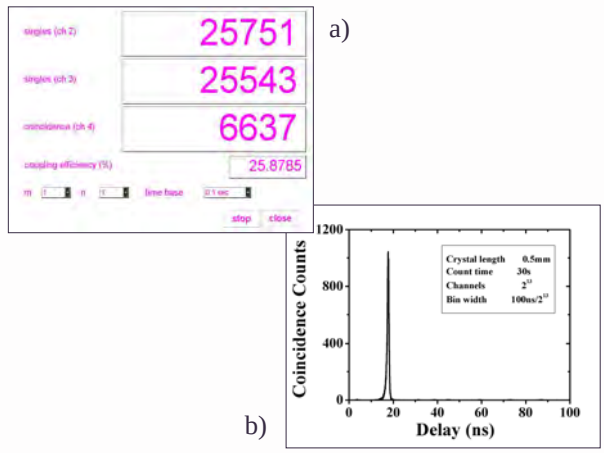

Figure 10. a) Print-screen showing the singles and coincidence rates in the experiment with a Type-II SPDC. The maximum overall efficiency obtained was 25.88%. Assuming detector QE∼50% and filters transmission coefficients of 90% we can estimate a coupling efficiency of around 58%. The coincidences rate is ∼265 cps/mm(BBO)/mW(pump). b) MCA output.

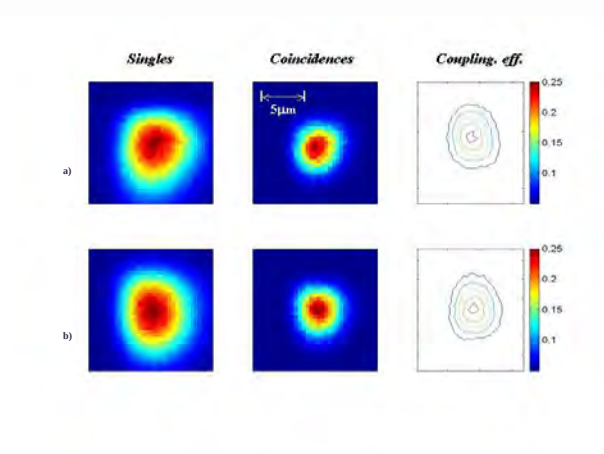

Figure 11. Scans of the singles and coincidence count rates. The a) and b) correspond to the case when the left and the right fiber respectively were maintained fixed.

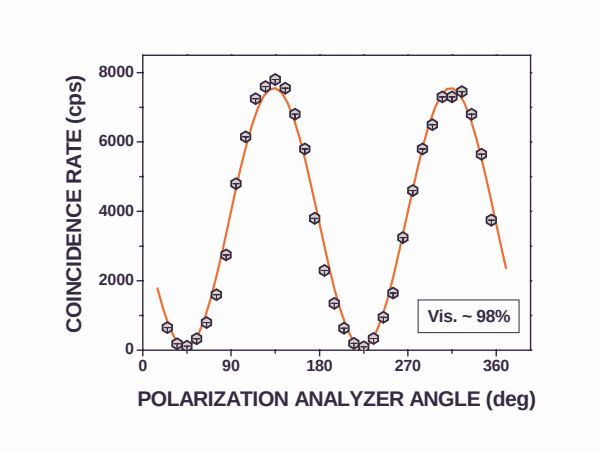

Figure 12. Coincidence rate behavior in function of one polarization-analyzer angle while the other is set at 45 deg. The visibility of the sinusoidal modulation is ∼98% and the overall coupling efficiency is ∼17%.

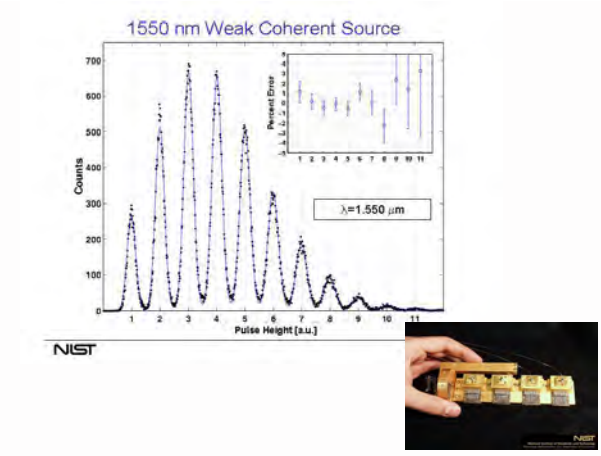

Figure 13. Photon number distribution (black dots) for a weak pulsed laser. The expected compound Poisson distribution is shown as solid line. In the corner the four number-photon resolving counting devices used at the Quantum Imaging Lab, Boston University.

use in a quantum-optical system at wavelengths from 2 μm to 200 nm. Each photon counter comprises a small square (20μm $\times$ 20μm) of tungsten deposited on a standard silicon wafer and cooled using an adiabatic-demagnetization refrigerator. Exploiting the sharp superconducting-to-normal resistive transition of tungsten at 100 mK, these TES single-photon counters output a current pulse that is proportional to the cumulative energy in an absorption event. This proportional pulse-height enables the determination of the energy absorbed by the TES with a resolution of ∼0.3 eV FWHM. For IR/optical photons of energy ∼1 eV, this resolution allows the direct conversion of sensor pulse-height into photon number. Fig. 13 shows a pulse-height spectrum from the output of a pulsed laser. Each peak corresponds to the absorption of a discrete number of photons in the detector, illustrating the Poissonian statistics of the photon arrivals. The number-photon resolving detectors have been also tested at the Quantum Imaging Laboratory with SPDC entangled photons. The inset of Fig. 14 shows the cryogen with the four detectors on the optical table where was the SPDC generation. Fig. 14 shows a typical photon energy distribution taken in one of the experiment, in which either one or two photons can

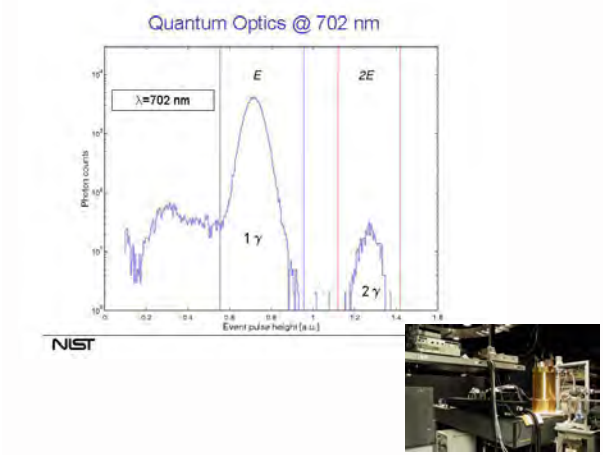

Figure 14. Logarithmic-scale histogram of photon energy in a typical experiment to detect down-converted light with a transition-edge sensor. The peak on the left, labeled E, registers single-photon events, while the peak on the right, labeled 2E, registers double-photon events.

reach the TES. The spectrum in Fig. 14 shows two regions of interest, peaks centered at a lower energy E and a higher energy 2E. The area under the lower-energy peak gives the number of single-photon detection events registered, while the area under the higher-energy peak gives the number of two-photon events. Since the SPDC photons used in this experiment are quasi-monochromatic, we can exploit the energy-resolving capability of the TES detectors to resolve one- and two-photon wave packets at rates of up to 30 kHz. In order to avoid spurious "pileup" counts, the experiments were performed with count rates an order of magnitude lower. If our source of light produced pulses of photon number N, Fig. 14 would feature a peak centered at NE.

4. CONCLUSION

We have shown polarization-entangled photon sources for quantum key distribution (QKD). We have obtained a better coupling efficiency of down-converted photons into optical single-mode fiber with a high degree of polarization entanglement. The detection has been performed using commercially available Silicon avalanche photodiodes (APD) as well as using a novel photon-number-resolving cryogenic photodetector. *Acknowledgments* This work was supported by DARPA QuIST and NSF.

REFERENCES

1. A. V. Sergienko, M. Atatre, Z. Walton, G. Jaeger, B. E. A. Saleh, and M. C. Teich, "Quantum cryptography using femtosecond-pulsed parametric down-conversion," *Phys. Rev. A* **60**, p. R2622, 1999.
2. D. N. Klyshko, *Photons and Nonlinear Optics*, Gordon and Breach, New York, 1988.
3. A. Yariv, *Quantum Electronics*, Wiley, New York, 1975.
4. M. Atatre, G. D. Giuseppe, M. D. Shaw, A. V. Sergienko, B. E. A. Saleh, and M. C. Teich, "Multiparameter entanglement in femtosecond parametric down-conversion," *Phys. Rev. A* **65**, p. 023808, 2002.
5. M. Atatre, G. D. Giuseppe, M. D. Shaw, A. V. Sergienko, B. E. A. Saleh, and M. C. Teich, "Multiparameter entanglement in quantum interferometry," *Phys. Rev. A* **66**, p. 023822, 2002.
6. B. E. A. Saleh, A. F. Abouraddy, A. V. Sergienko, and M. C. Teich, "Duality between partial coherence and partial entanglement," *Phys. Rev. A* **62**, p. 043816, 2000.
7. A. F. Abouraddy, B. E. A. Saleh, A. V. Sergienko, and M. C. Teich, "Entangled-photon fourier optics," *J. Opt. Soc. Am. B* **19**, p. 1174, 2002.